Experimental demonstration and visual observation of dust trapping in an electron storage ring

Yasunori Tanimoto,* Tohru Honda, and Shogo Sakanaka

Accelerator Laboratory, High Energy Accelerator Research Organization (KEK), Oho, Tsukuba, Ibaraki 305-0801, Japan

(Received 17 June 2009; published 16 November 2009)

Sudden decreases in the beam lifetime, which are attributed to the dust trappings, sometimes occur at the electron storage ring Photon Factory Advanced Ring (PF-AR). Since these dust events cause difficulties in user operations, we have been carefully observing this phenomenon for many years. Our observations indicated that the dust trappings could be caused by electric discharges in vacuum ducts. In order to demonstrate this hypothesis experimentally, we designed a new vacuum device that intentionally generates electric discharges and installed it in PF-AR. Using this device, we could repeatedly induce sudden decreases in the beam lifetime because of the generated electric discharge. We also detected decreases in the beam lifetime caused by mechanical movement of the electrodes in the device. Moreover, we could visually observe the dust trapping phenomenon; the trapped dust particle was observed by two video cameras and appeared as a luminous body that resembled a shooting star. This was the first direct observation of a luminous dust particle trapped by the electron beam.

DOI: 10.1103/PhysRevSTAB.12.110702 PACS numbers: 29.27.Bd, 29.20.db, 52.80.Vp, 94.30.Hn

I. INTRODUCTION

The phenomenon of the decrease in the beam lifetime during accelerator operations has been observed in many electron storage rings [1–9]. Such irregular beam losses sometimes last for a few minutes or occasionally for several hours. These events are attributed to the trapping of positively charged microparticles (dust) in the electron beams on the basis of the following circumstantial evidences: (1) the decrease in the beam lifetime is often accompanied by a burst of γ rays detected ahead of the beam direction [2,3,7,8,10], and (2) such a decrease does not occur or is transient in accelerators that store positron beams [3,7–9,11]. Some theoretical models on the dust trapping have been developed previously [4,5,12–14], and they support the observations. However, knowledge on the dust trapping phenomenon is limited because of the lack of the sufficient resources for investigating this phenomenon as well as the difficulty in reproducing the dust trapping experiments.

The Photon Factory Advanced Ring (PF-AR) at the High Energy Accelerator Research Organization (KEK) is a 6.5-GeV electron storage ring operated for the synchrotron radiation (SR) research. The principal parameters of the PF-AR are shown in Table I. The PF-AR routinely stores single-bunch electron beams with a maximum beam current of 60 mA. Routine operations of the storage ring are sometimes disturbed by sudden decreases in the beam lifetime [2,15]; these disturbances are not only due to the reduced beam lifetime but also due to bursts of γ rays, because of which the radiation intensity in the experimental area sometimes increases. Thus, mitigation of the decreases in the beam lifetime is one of the most important issues that needs to be addressed for enabling stable user operations at PF-AR.

Previously, it was suggested that distributed ion pumps (DIPs) installed in the vacuum chambers for dipole or

TABLE I. Principal parameters of the PF-AR.

Beam energy	6.5 GeV
Injection beam energy	3.0 GeV
Initial stored current	60 mA
Circumference	377 m
Natural beam emittance	293 nm rad
Natural rms bunch length	17 mm at 6.5 GeV
Harmonic number	640
Number of bunches	1 (single-bunch operation)
rf frequency	508.6 MHz
Revolution frequency	795 kHz
Betatron tunes	10.15 (horizontal), 10.21 (vertical)
Critical energy of SR	26 keV
Electron bunch population	4.71×10^{11} electrons/bunch at 60 mA
Beam lifetime	20–23 hours[a] at 60 mA
Ring-averaged dynamic pressure	3.2×10^{-7} Pa at 60 mA
Ring-averaged static pressure	2.0×10^{-8} Pa
Main vacuum pumps	TSP × 184, DIP × 56, SIP × 111[b]
Main beam duct material	OFHC[c] Cu (6 mm thick)

[a]Beam lifetime in SR user operations depends on in-vacuum undulator gaps.
[b]TSP: titanium sublimation pump; DIP: distributed ion pump; SIP: sputter ion pump.
[c]OFHC: oxygen-free high conductivity.

*yasunori.tanimoto@kek.jp

quadrupole magnets were the source of dust [9,16–18]. To decrease the effect of the generated dust on the beam lifetime, an inverted-type DIP with grounded anodes and negatively charged cathodes was tested at PETRA [19]. The results suggested that inverted-type DIPs were useful in mitigating the decreases in the beam lifetime. At PF-AR, we replaced all the DIPs in 56 dipole magnet chambers by inverted-type ones during the major upgrade of the machine in 2001. Contrary to our expectations, the polarity inversion of the DIP was not effective at PF-AR.

Over the ensuing years, the decreases in the beam lifetime continued to occur. From November 2007, we switched all the DIPs off during user operations in order to estimate their contribution upon the decreases in the beam lifetime. As a result, the frequency of such events was reduced (DIP-ON: 0.22 times/day; DIP-OFF: 0.15 times/day) [15]. However, the decreases in the beam lifetime were still observed.

Continuous observations of these events in PF-AR suggested that harmful dust particles were produced not only by the DIPs but also by electric discharges in the vacuum chambers. The latter hypothesis was supported by the fact that, when the decrease in the beam lifetime occurred, a momentary increase in vacuum pressure in the in-vacuum undulators (vertical gap: 10 mm) or the radio frequency (rf) kicker with stripline electrodes for the fast feedback system was observed. The possibility of dust production by sparking at the electrostatic separators [4] or at the rf-contact fingers [17] was also reported.

In general, owing to the high bunch current and short bunch length, strong electric fields can be induced at the chamber walls with the passage of a bunch. In the case of the PF-AR, the instantaneous electric field is estimated to be 2.9 MV/m at the bottom of the smooth racetrack-shaped chamber (width: 90 mm; height: 34 mm) at an average beam current of 60 mA (single bunch) and an rms bunch length of 17 mm. If there are sharp edges on the walls such as the corner of the pumping ports, the high electric fields can induce discharges in the chamber and consequently may produce dust.

In order to prove the hypothesis that the said electric discharges, namely discharges caused by high voltage (HV) applications and beam-induced electric fields, result in dust trapping, we carried out research using a unique discharge device installed in a long straight section of the PF-AR. In our experiments, we intentionally generated dust particles by electric discharge and observed how they affect the stored beams. We expect our experimental results to be useful in investigating the characteristics of the dust trapping phenomenon.

II. EXPERIMENTAL ARRANGEMENT

A. Discharge device

On the basis of the hypothesis that electric discharges induce a decrease in the beam lifetime, the discharge device was designed to simulate similar natural events in the vacuum chambers of the storage ring. In order to generate two types of electric discharges near the stored beams, the device was equipped with two types of retractable electrodes, as described below. The image of the interior of the discharge device is shown in Fig. 1. Schematic representations of the device chamber and retractable electrodes are shown in Figs. 2 and 3, respectively.

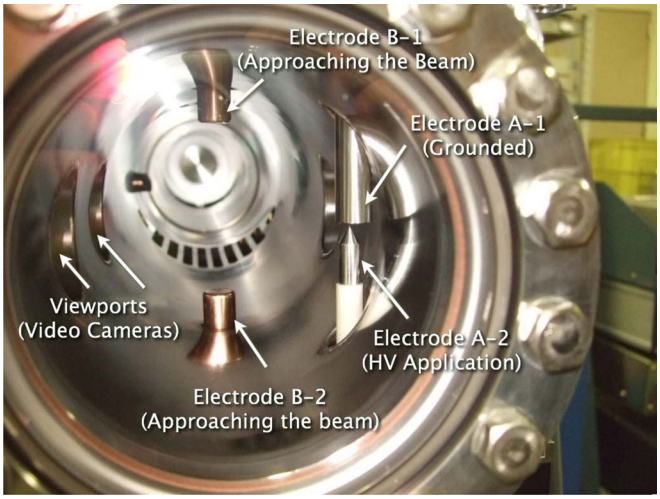

FIG. 1. (Color) Image of the interior of the discharge device. Electron beams pass from the front port to the back port.

Electrodes A.—To simulate electric discharges in the DIPs, a pair of movable electrodes was located at the side of the beam orbit (Fig. 3, left). DC HVs of up to ± 7.5 kV were applied to the lower electrode (A-2), which was made of stainless steel and covered by an alumina ceramic sleeve. The tip of A-2 was made of titanium. The opposite electrode (A-1) was grounded and made of titanium-coated stainless steel. Two different power supplies were used to apply negative (maximum current: 5 mA) or positive (maximum current: 25 mA) HV.

Electrodes B.—To simulate discharge-prone vacuum chambers such as rf kickers, in-vacuum undulators, and movable beam scrapers, a pair of grounded electrodes that could be moved vertically toward the stored beams was installed above and below the beam orbit (Fig. 3, right). Each electrode rod was cooled by water and its base was electrically shielded by rf-contact fingers in order to reduce temperature increase caused by beam-induced rf fields. Both electrode rods were made of copper; the tips of the upper (B-1) and lower (B-2) electrodes were made of aluminum and copper, respectively. Electric discharge events due to beam-induced fields were expected to occur when these electrodes were brought to the vicinity of the beams.

Each electrode was remotely operated during the dust trapping experiments and retracted into the initial position during the user operations. The vacuum chamber of the

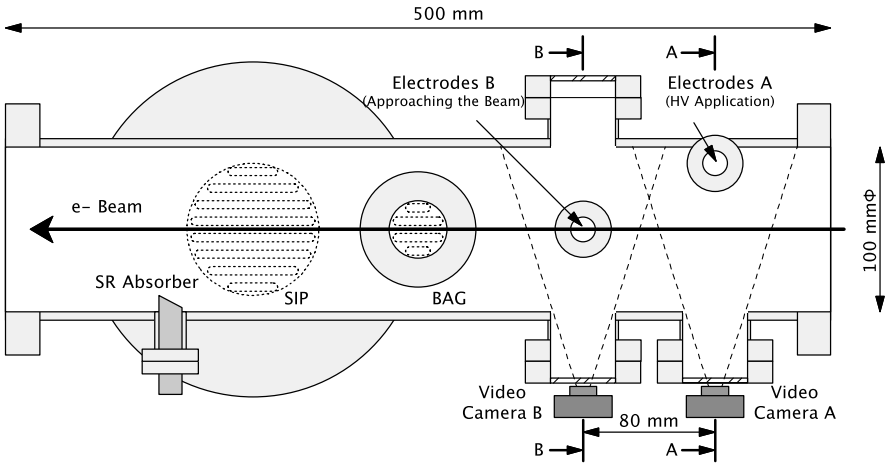

FIG. 2. Schematic representation of the discharge device chamber.

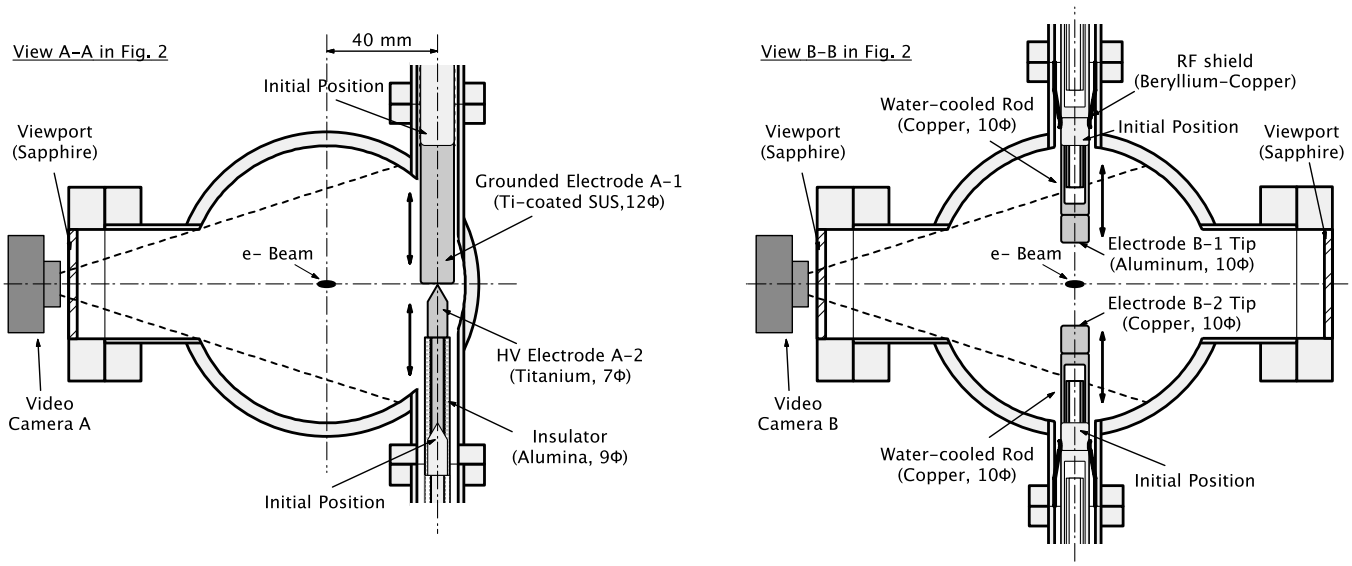

FIG. 3. Schematic representations of two types of electrodes. Electrodes on the left are used for the electric discharges caused by the applied DC HVs, and those on the right are used for the electric discharges caused by beam-induced rf fields.

discharge device was made of stainless steel. The tips of all the electrodes were exchangeable, because of which the dependence of the harmful dust generation on the electrode materials can be investigated in the future.

B. Monitoring instruments

In order to detect the sparks formed at electrodes A and B, two video cameras (KPC-S700CHBA with Sony Super HAD CCD) were attached to the sapphire viewing ports of the discharge device. Electrodes A and B were monitored by cameras A and B, respectively. The longitudinal distance between these two cameras was 80 mm. The visual fields of these cameras are indicated by the dashed lines in Figs. 2 and 3. Movies with sound were recorded on hard disk drives at the rate of 30 frames/s. A Bayard-Alpert gauge (BAG) was installed in the device chamber to detect increases in the vacuum pressure at the discharge.

Two radiation detectors (ALOKA MAR-782, silicon semiconductor type) were installed at different locations on the extension lines from the two straight sections, as shown in Fig. 4. One of the radiation detectors, RD#1, was located on the extension of the south long straight section where the discharge device was installed. RD#2 was located on the extension of the next short straight section, which was separated from the long straight section by two bending magnets. To reduce predominant x-ray backgrounds from SR, the detectors were shielded by 60-mm-thick lead blocks. These detectors could be used to monitor the bremsstrahlung caused by collisions between the stored beams and the trapped dust particles.

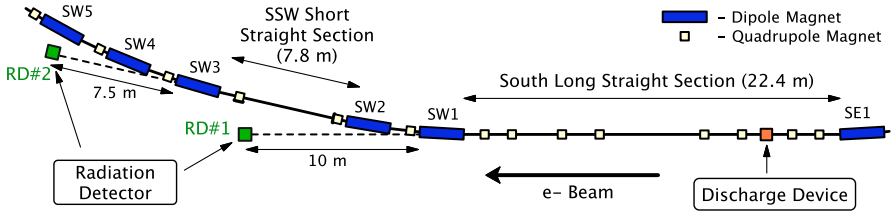

FIG. 4. (Color) Layout of the experimental setups in the PF-AR storage ring.

C. Beam current, lifetime, and beam loss rate

The beam current was measured by a DC current transformer installed in the ring and recorded every 0.6 s in a data server. The resolution (standard deviation) of the measured beam currents was typically 4 μA.

The beam lifetime, defined as a reciprocal of the exponential current-decay constant, was calculated by applying a linear least-squares fitting to the beam current change with time on a semilog graph. In order to reduce dispersion in the calculated beam lifetimes, the number of current data values used in each lifetime calculation was chosen as 180, i.e., the beam lifetime was obtained from beam currents recorded in the past 108 s.

The beam loss rate, i.e., the beam current decrease in unit time, was calculated by applying a linear least-squares fitting to the current decrease with time. To express rapid changes in the beam current, the number of current data values used in each calculation was chosen as 30, i.e., the loss rate was a gradient of the current decay in the past 18 s. The current decay rate was converted to the decay rate of the number of electrons by multiplying it with a coefficient, 7.85×10^9 electrons/mA.

III. EXPERIMENTAL RESULTS

A. Dust production experiments by applying HV to the electrodes

We carried out dust production experiments using the designed discharge device in the PF-AR. In all our experiments, we used the same machine parameters as those used during the user operations (see Table I).

First, we used electrodes A for the dust production by HV applications. The vertical gap between electrodes A-1 and A-2 was adjusted by moving them simultaneously so that the center of the gap was at the beam level. After reducing the gap to 1 mm, a DC HV was applied to the lower electrode A-2, and the gap was repeatedly reduced in 0.2-mm steps until electric discharge occurred. Sparks produced at the electric discharge events were detected by video camera A, and increases in the vacuum pressure were observed by the BAG. An example of the spark detected by the camera is shown in Fig. 5. In this case, a DC HV of -5.0 kV was applied.

One experimental result obtained with a negative HV application is shown in Fig. 6. In this experiment, we

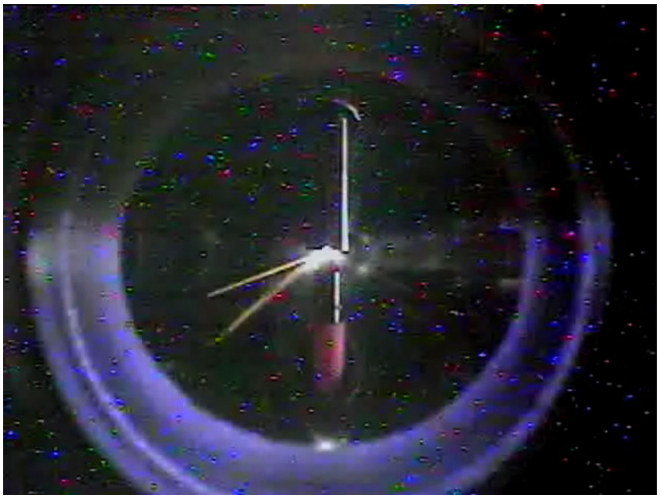

FIG. 5. (Color) Image of a discharge event. In this case, the spark is generated by applying a DC HV of -5.0 kV to the lower electrode.

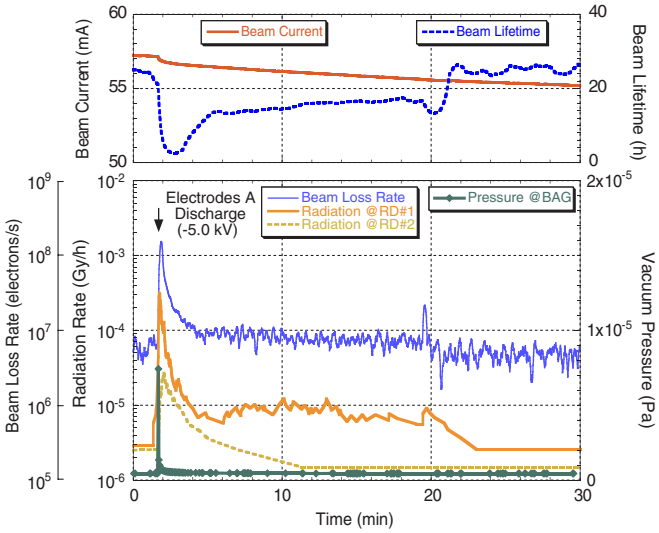

FIG. 6. (Color) Experimental data recorded when the beam lifetime decreased because of electric discharge. The discharge was artificially induced by applying a DC HV of -5.0 kV at the time indicated by the arrow. Upper graph: beam current and beam lifetime; lower graph: beam loss rate, radiation intensity, and vacuum pressure.

generated the electric discharge with a DC HV of −5.0 kV at the time indicated by the arrow in Fig. 6. Immediately after the discharge generation, the beam lifetime began to decrease. Simultaneously, an increase in the radiation intensity was observed by the two detectors, and an instantaneous increase in the vacuum pressure was observed by the BAG.

On the basis of the results shown in Fig. 6, the following could be stated: (1) the increase in the vacuum pressure was transient, whereas the decrease in the beam lifetime lasted for approximately 18 min, i.e., the reduced lifetime was not attributed to the increase in the vacuum pressure, and (2) the beam loss rate had a good proportional relation with the γ-ray intensity at RD#1 (on the extension of the south long straight section) as illustrated in Fig. 7; this means that the beam loss was mainly caused by obstacles in the long straight section. Therefore, it was concluded that the dust was produced by electric discharge and then trapped by the beams.

We could induce similar dust trapping events by applying a positive HV of +7.5 kV. The experimental results obtained in this case are shown in Fig. 8, which illustrates the decrease in the beam lifetime could be repeatedly induced by electric discharge. Owing to the same reasons stated above, the observed decreases in the beam lifetime in this experiment were thought to be caused by the dust events. On the basis of the fact that we could induce the

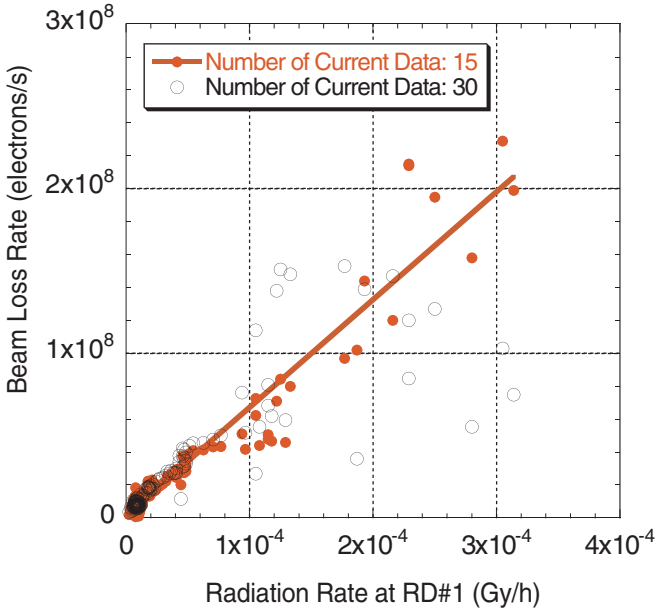

FIG. 7. (Color) Correlation between the beam loss rate and the γ-ray intensity at RD#1. A good proportion is confirmed by the plot of the red closed circles, where the beam loss rate was calculated with a smaller number (15, usually 30) of current data in order to reduce time lags in the regime where the beam loss rate changed rapidly. The black open circles are additionally plotted using the same data as those in Fig. 6; the proportional relation appears worse due to large time lags.

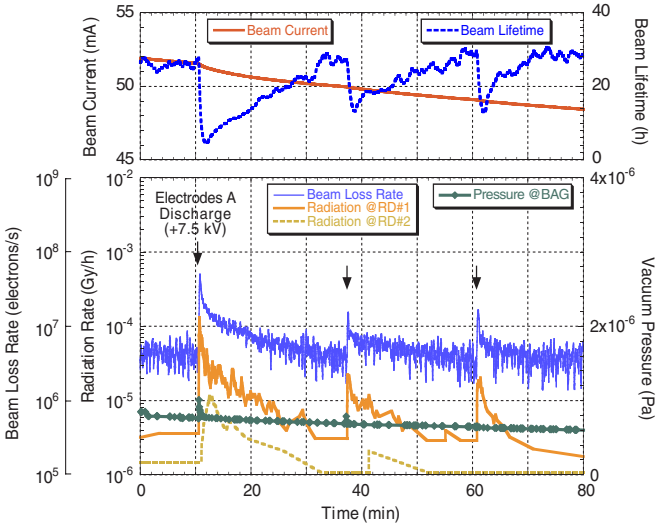

FIG. 8. (Color) Experimental data recorded when the beam lifetime repeatedly decreased because of electric discharge. The discharges were artificially induced by applying DC HVs of +7.5 kV at the time indicated by the arrows.

decreases in the beam lifetime by positive and negative HV applications, we concluded that the polarity of the applied HV was not essential for the occurrence of the decreases in the beam lifetime. This supported our experience on the DIPs at PF-AR.

B. Dust production experiments by bringing electrodes close to beams

Next, we used electrodes B for the dust production experiments, in which we intentionally induced electric discharges by shifting electrodes B-1 and B-2 simultaneously or individually to the vicinity of the electron beam.

In one experiment, when the tip of the lower electrode B-2 reached a point 22 mm away from the beam, weak green light emissions were repeatedly observed near the base of the electrode; this was accompanied by a slight increase in the vacuum pressure. Simultaneously, a decrease in the beam lifetime and an increase in the radiation intensity were observed, as shown in Fig. 9. Also in this experiment, the increase in the vacuum pressure was transient, whereas the increase in the radiation intensity at RD#1 was lasting. These observations indicated that this decrease in the beam lifetime was attributed to dust trapping. From this experiment, it was shown that harmful dust particles could be produced by beam-induced discharge. Unlike the electric discharges caused by the DC HV applications, this discharge lasted for a few seconds. Hence, it might be a multipactor discharge caused by beam-induced rf fields.

In this experiment, we observed a time lag between the radiation bursts at the two detectors. At RD#1, the radiation burst commenced at approximately the same time as the onset of the decrease in the beam lifetime. Two minutes later, the radiation intensity at RD#1 began to decrease,

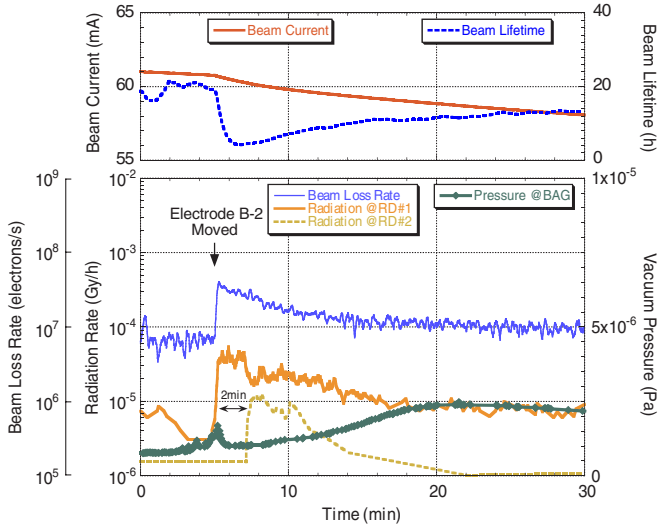

FIG. 9. (Color) Experimental data recorded when the beam lifetime decreased because of electric discharge caused by beam-induced rf fields. The discharge was artificially induced by bringing electrode B-2 to the vicinity of the electron beam at the time indicated by the arrow. The decrease in the beam lifetime lasted for 98 min in this experiment (not shown in the figure).

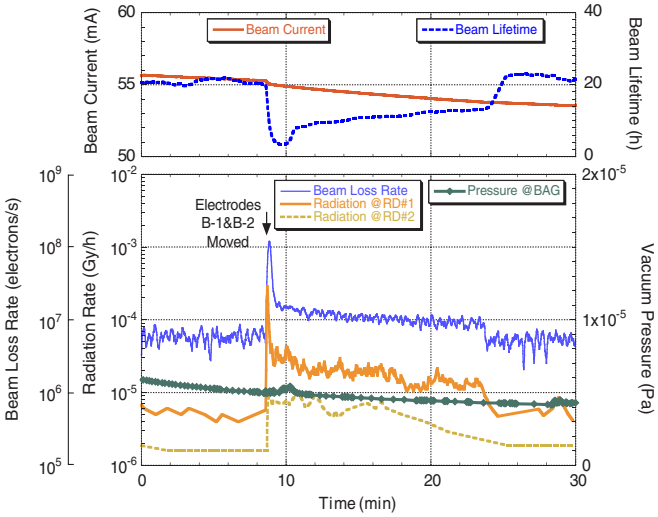

FIG. 10. (Color) Experimental data recorded when the beam lifetime decreased because of the mechanical movement of electrodes B. Appearance of a luminous body was observed concurrently with the decrease in the beam lifetime using video cameras.

whereas that at RD#2 began to increase. This suggested that the dust particles traveled longitudinally and passed through the bending magnets while being trapped by the beam. Although such a behavior was not always observed in our experiments, similar observations have been reported previously [3,10,20,21].

Temperature increases were observed when electrodes B were brought close to the beams. The temperature measured on the surface of the outside wall of the electrode port exceeded 100°C when the distance between the electrode tip and the beam was less than 20 mm. Therefore, the minimum distance between the electrode tip and the beam was set to 20 mm. As shown in Fig. 9, a gradual increase in the vacuum pressure caused by the temperature increase was observed while the distance was kept at 22 mm. On the other hand, no significant increase in the temperature was observed during the experiments performed using electrodes A.

C. Visual observation of luminous bodies

In a certain case, concurrently with a sudden decrease in the beam lifetime, we observed a luminous body repeatedly traversing the beam orbit like a shooting star. The luminous body was observed by both video cameras.

This phenomenon appeared in the experiment performed using electrodes B. Immediately after electrodes B-1 and B-2 were simultaneously shifted from their initial positions (distance between each electrode and the beam was 50 mm) by 10 mm, the beam lifetime suddenly decreased, and a radiation burst was detected at RD#1, as shown in Fig. 10. Then, the decrease in the beam lifetime and the increase in the radiation intensity at RD#1 lasted for approximately 15 min. No spark nor vacuum pressure increase was observed at the commencement of the decrease in the beam lifetime. These observations suggested that dust was generated by the mechanical movement of the electrodes without any electric discharge and trapped continuously in the beam.

When the beam lifetime began to decrease, the luminous body appeared 9 times within duration of 6 s and then disappeared. From the movies recorded during this event (see Video 1), frames in which the trace of the body could be recognized were extracted and summarized in Fig. 11. The luminous body repeatedly appeared as a clear horizontal line on the beam orbit or as a dot, whereas the chamber walls were dimly illuminated by the scattered SR. The images in the right and left columns in the frame

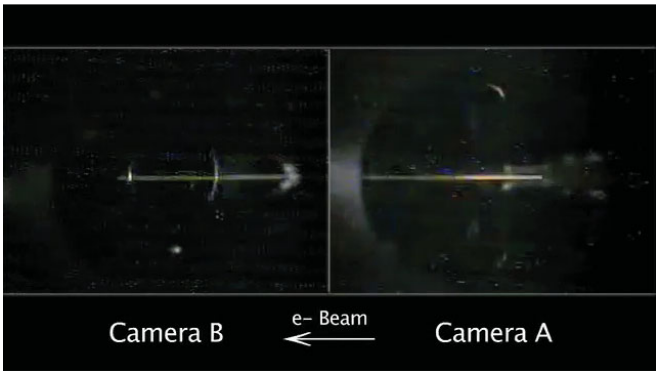

VIDEO 1. Movies recorded by video cameras A and B during the dust production experiment. The images in Fig. 11 were extracted from these movies.

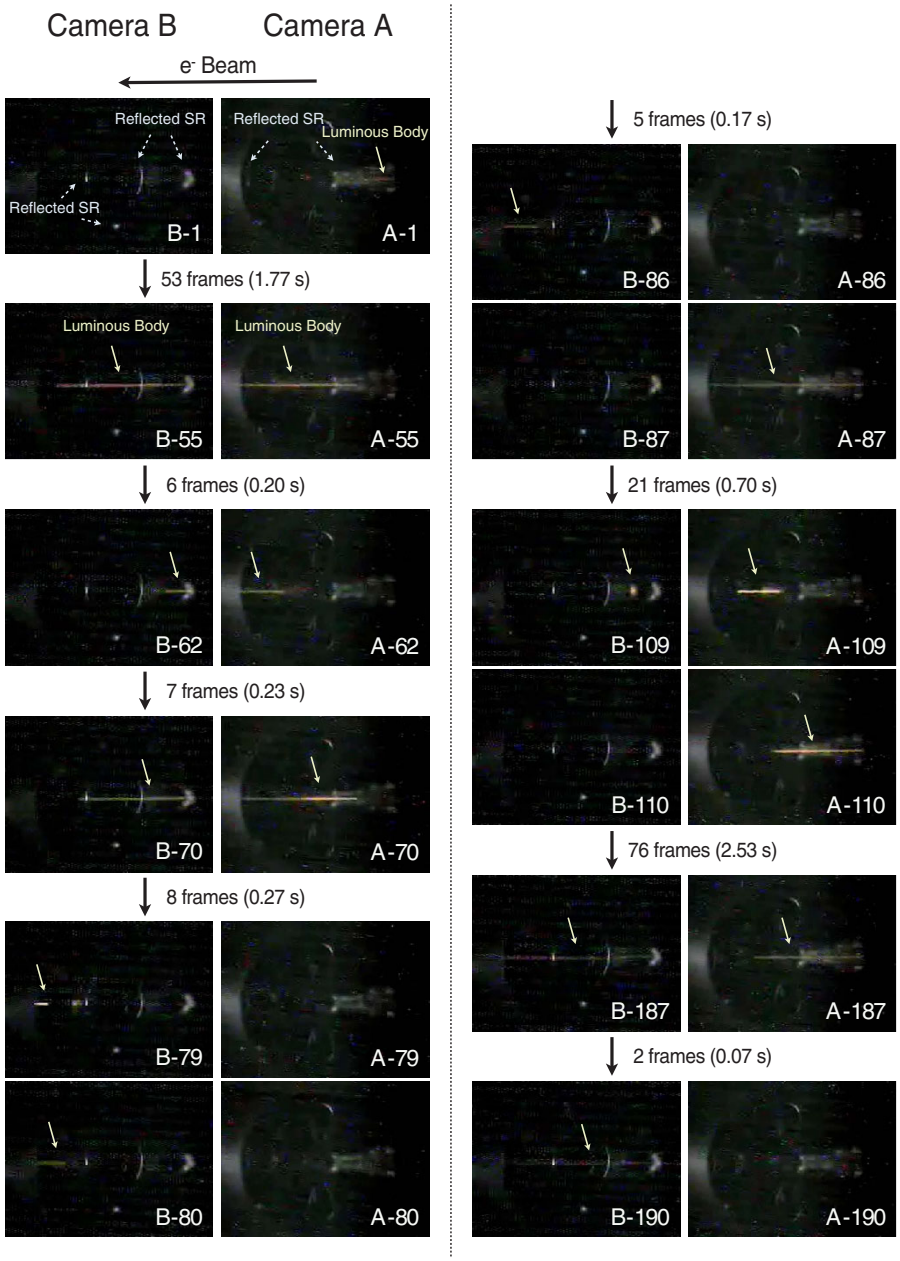

FIG. 11. (Color) Frame-by-frame images selected from the recorded movies. The luminous bodies observed during the experiment are indicated by the arrows.

stream are those recorded with cameras A and B, respectively. We labeled each image with an index number upon the first appearance of the luminous body. The time interval between two consecutive frames was approximately 33 ms.

Since the movies were independently recorded by the two video cameras, we attempted to synchronize these movies by the following procedure. We first noticed images A-55 and B-55 in Fig. 11, both of which showed the first clear traces of the luminous body, and assumed that these frames should coincide within a frame interval of 33 ms. Subsequently, we found that most of the subsequent traces recorded by both the video cameras were synchronized within one or two frames. Then, we considered this synchronization to be sufficiently reliable. After the synchronization, we found that the intervals between the consecutive appearances of the luminous body were not constant and ranged from 0.07 to 2.53 s, as summarized in Table II.

IV. DISCUSSIONS

A series of our experiments ascertained that the sudden decrease in the beam lifetime was induced by the following processes: (i) electric discharges caused by the applied DC HVs and the beam-induced rf fields; (ii) mechanical movement of the electrodes in the vacuum device.

TABLE II. Summary of the repeated appearance of the luminous body, which appeared 9 times in 6 s. For each appearance, the observed position (denoted as ''Obs.'') and time interval from the previous appearance are listed.

Appearance number	Observed position Camera B	Camera A	Interval from previous appearance (s)
1		Obs.	···
2	Obs.	Obs.	1.77
3	Obs.	Obs.	0.20
4	Obs.	Obs.	0.23
5	Obs.		0.27
6	Obs.	Obs.	0.17
7	Obs.	Obs.	0.70
8	Obs.	Obs.	2.53
9	Obs.		0.07

The polarity of the applied HVs and the source of the electric discharge (applied DC HVs or beam-induced rf fields) did not play a major role in dust production. Although the decrease in the beam lifetime was not always induced by every electric discharge, the dust events were well reproduced.

The candidates for the trapped dust particles in our experiments were materials of the electrodes or the rf contact, i.e., copper, aluminum, titanium, stainless steel, or beryllium copper, or possibly, other kinds of dust that had previously adhered to the electrodes. Since it was difficult to identify the dust species in our experiments, we expect that the exchange of the electrode tips will provide some information about the dependence of the harmful dust generation on the electrode materials.

Now, we discuss the identity of the luminous body. As shown in Fig. 10, the radiation intensity at RD#1 was almost proportional to the beam loss rate, which was confirmed by a similar plot to Fig. 7, and there was no significant change in the vacuum pressure; this indirectly showed that the beam losses during this event were mainly caused by obstacles in the long straight section. Furthermore, when the luminous body was visually observed for 6 s, the radiation intensity at RD#1 also showed an instantaneous peak ($> 1 \times 10^{-4}$ Gy/h for 7 s). On the basis of these observations, we concluded that the luminous body was nothing but the trapped dust. This is the first direct evidence of dust trapping in the beam.

As shown in Fig. 11, the trapped dust is mostly observed simultaneously by two separate cameras. This confirms that the trapped dust moves longitudinally. The longitudinal speed of the trapped dust particle (or particles) is roughly estimated. In the case of higher speed, we noticed images A-55 and B-55 in Fig. 11. The luminous dust particle might travel a distance of more than 200 mm (maximum visual field of the cameras is approximately 100 mm each) within one frame (33 ms). Then, the estimated longitudinal speed is more than 6 m/s. In the case of lower speed, we noticed images B-79 and B-80. The dust particle might travel a distance of approximately 20 mm in two frames (66 ms). Then, the estimated longitudinal speed is 0.3 m/s. In another case, as shown in image B-109, the dust particle appears at considerably lower speed.

As summarized in Table II, the time interval between consecutive appearances of the luminous body ranges from 0.07 to 2.53 s. The trapped dust cannot circulate the storage ring in such short intervals. Therefore, it is reasonably assumed that a single luminous dust particle oscillates longitudinally near the observed region. However, the fact that the intervals were not periodic shows that the oscillation was not simple harmonic. In addition, we cannot rule out other possibilities: (1) several luminous dust particles were produced simultaneously, or (2) a large dust particle was split into several fragments after it was trapped by the beam.

There are three possible reasons for the emission of light from a trapped dust particle: (1) spontaneous radiation caused by high temperatures, i.e., blackbody radiation, (2) scattering of visible SR, and (3) light emission from an insulator or a semiconductor under electron beam irradiation, i.e., cathodoluminescence. In this experiment, we presume the dust to be a metal particle because it was most probably a fragment of the electrode-B components. Therefore, we consider that the blackbody radiation and the scattering of SR are more prevailing processes than the cathodoluminescence. We investigated whether the light emission from the dust was strong enough to be visually observed by our CCD cameras if the blackbody radiation and the scattering of SR were assumed.

The intensity of the visible light incident on the CCD camera, as the number of photons per unit time, was roughly estimated for each process by taking account of the solid angle of the CCD camera. For the blackbody radiation, we assumed the dust to be a spherical perfect blackbody, and calculated the photon intensities by integrating visible light spectra derived from the Planck's radiation law. For the scattering of visible SR, we considered the Mie scattering by a homogeneous sphere, and calculated the photon intensities using the program MiePlot [22] based on the BHMIE algorithm that calculates the scattering coefficients [23]. The photon intensity incident on the particle was assumed to be the visible light component (380–780 nm) of the direct SR from the bending magnet, and the scattering intensity in the 90-degree direction was computed assuming the wavelength of all the incident photons to be 555 nm for simplicity. Although the intensity of the Mie scattering depends on the refractive index of the sphere, we temporarily used the refractive index of copper in this calculation.

The calculation results are illustrated in Fig. 12 as functions of particle diameter within a range of 0.1 to 100 μm. The photon intensity of the blackbody radiation is proportional to the square of the particle diameter. The intensity of the Mie scattering is also proportional to the

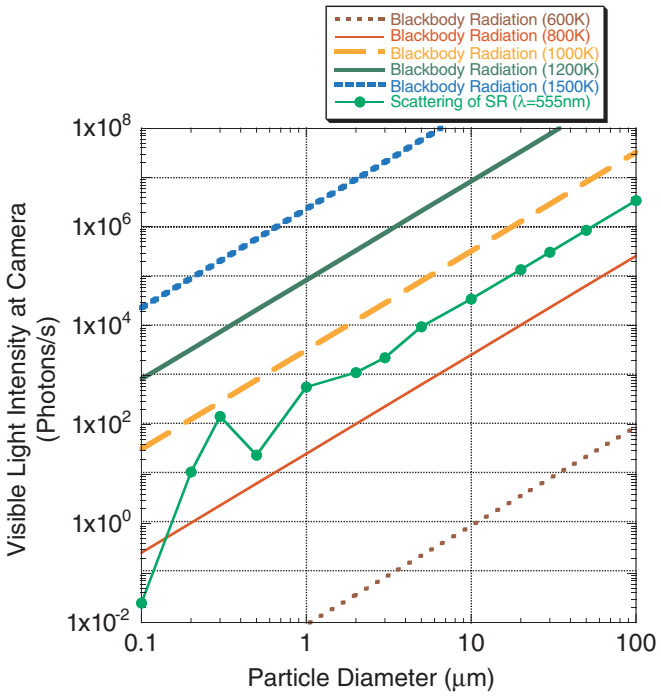

FIG. 12. (Color) Estimation results of visible-light intensities at the camera as functions of dust diameter. The photon intensities were calculated under two kinds of light emission processes, blackbody radiation, and scattering of SR.

square of the particle diameter in the regime where the diameter is larger than the wavelengths of visible light.

For general use, our CCD camera needs a minimum subject illumination of about 1 lx. Assuming a point light source and ideal focusing, this sensitivity is equivalent to the order of 10^3 photons/s on one pixel of the CCD. However, we used the video camera with a fixed-focus lens, and the image from the point light source could spread out over a number of pixels on the CCD. In this case, the required photon intensity should be 1 or 2 orders of magnitude higher than 10^3 photons/s.

As shown in Fig. 12, the photon intensity by the blackbody radiation with the temperature higher than about 1000 K is estimated to exceed the intensity by the SR scattering. In the case of blackbody radiation, the temperature of the dust should reach at least 800 or 1000 K for the visual observation. If the temperature of a dust becomes as high as 1500 K, even the dust whose diameter is submicron could be observed with enough brightness. It has been predicted that the temperature of the trapped dust particles can increase considerably upon their interaction with the stored beams [4,5,13,14], and in certain conditions, the temperature was calculated to reach approximately 1500 K [13,14]. Therefore, we consider that it is quite possible to observe a microdust by the blackbody radiation. In our experimental condition, the scattering of SR by a dust particle is too dark to be visually observed if the diameter is as small as 1 μm. On the other hand, the dust whose diameter is much larger than 10 μm could be visually observed by the scattering of SR, even if its temperature is lower than 800 K. In any case, further investigation such as spectral measurements of the emitted light is necessary to confirm this.

We succeeded in the visual observation only once despite several tens of the dust-generation experiments. Then, we presume that the trapped dust particles can be visually observed only under certain conditions. The mass of the dust particle was expected to be one of the most important factors because the radiation intensity at RD#1, which was closely related to the mass of the trapped dust particle, immediately decreased when the luminous dust disappeared, as mentioned above. Moderately heavy dust particles, therefore, could be more suitable for visual observation. The trapped dust particles generated by the electric discharges were not detected by the video cameras so far.

If a method for generating visible dust particles more frequently is established, further experiments with reinforced equipment can be performed. For example, fine time-resolution measurements using high-speed cameras or time-of-flight measurements using photomultipliers will enable a more precise investigation of the behavior of the trapped dust particles.

V. CONCLUSIONS

A series of experiments performed using our dust-generation device demonstrated that sudden decreases in the beam lifetime could be repeatedly triggered by electric discharges generated by the applied DC HVs (positive and negative) and beam-induced rf fields. In one of our experiments, dust trapping was induced by mechanical movement of the electrodes in the vacuum device. Furthermore, we found that the trapped dust could be visually observed under certain conditions. This observation is the first direct evidence for the dust particle being trapped by the electron beam and the longitudinal movement of the trapped dust particle.

ACKNOWLEDGMENTS

The authors are grateful to Dr. Y. Hori for useful comments and discussions on the dust trapping mechanism and the conceptual design of the discharge device. The authors are indebted to Mr. T. Uchiyama, Mr. T. Nogami, and engineers from Mitsubishi Electric System & Service Co., Ltd. for their help in preparing and installing the experimental devices.

[1] K. Huke, N. Kajiura, Y. Kamiya, N. Kanaya, T. Katsura, M. Kihara, H. Kitamura, H. Kobayakawa, M. Kobayashi, T. Koide, C. O. Pak, S. Sato, S. Shibata, T. Yamakawa, and Y. Yamazaki, IEEE Trans. Nucl. Sci. **30**, 3130 (1983).

[2] H. Saeki, T. Momose, and H. Ishimaru, Rev. Sci. Instrum. **62**, 874 (1991).
[3] P. Marin, Report No. LURE RT/91-03, 1991.
[4] D. Sagan, Nucl. Instrum. Methods Phys. Res., Sect. A **330**, 371 (1993).
[5] F. Zimmermann, Technical Report DESY HERA 93-08, 1993.
[6] G. Debut, J. M. Lefebvre, R. Morrison, I. Parat, J. Pelle, D. Schmied, and R. Souchet, in *Proceedings of the 4th European Particle Accelerator Conference, London, England, 1994* (World Scientific, Singapore, 1994), pp. 2473–2475.
[7] K. Kanazawa, S. Kato, Y. Suetsugu, H. Hisamatsu, M. Shimamoto, M. Sato, and M. Shirai, Appl. Surf. Sci. **169–170**, 715 (2001).
[8] U. Wienands, in *Proceedings of the 2001 Particle Accelerator Conference, Chicago, IL, 2001* (IEEE, Piscataway, NJ, 2001), pp. 597–601.
[9] Q. Qin and Z. Y. Guo, in *Proceedings of the 2nd Asian Particle Accelerator Conference, Beijing, China, 2001* (IHEP, Beijing, 2001), pp. 451–453.
[10] M. Kobayashi, Photon Factory Activity Report 1987, 66 (1988).
[11] M. Kobayashi, Y. Hori, and Y. Takiyama, Rev. Sci. Instrum. **60**, 1728 (1989).
[12] H. Saeki, T. Momose, and H. Ishimaru, Rev. Sci. Instrum. **67**, 1475 (1996).
[13] S. Heifets, Q. Qin, and M. Zolotorev, Phys. Rev. ST Accel. Beams **8**, 061002 (2005).
[14] A. Kling, in *Proceedings of the 10th European Particle Accelerator Conference, Edinburgh, Scotland, 2006* (EPS-AG, Edinburgh, Scotland, 2006), pp. 1486–1488.
[15] Y. Tanimoto, T. Honda, T. Uchiyama, and T. Nogami, Vacuum (to be published).
[16] Photon Factory Activity Report 1983/84, IV (1984).
[17] H. Saeki, T. Momose, and H. Ishimaru, Rev. Sci. Instrum. **65**, 3479 (1994).
[18] D. R. C. Kelly, Technical Report DESY HERA 98-02, 1998.
[19] K. Balewski, H. Ehrlichmann, J. Kouptsidis, and K. Wittenburg, in *Proceedings of the 5th European Particle Accelerator Conference, Sitges, Spain, 1996* (IOP, Bristol, 1996), pp. 436–438.
[20] H. Saeki, T. Momose, and H. Ishimaru, Rev. Sci. Instrum. **62**, 2558 (1991).
[21] D. R. C. Kelly, W. Bialowons, and K. Wittenburg, in *Proceedings of the 5th European Particle Accelerator Conference, Sitges, Spain, 1996* (IOP, Bristol, 1996), pp. 289–291.
[22] P. Laven, Appl. Opt. **42**, 436 (2003).
[23] C. F. Bohren and D. R. Huffman, *Absorption and Scattering of Light by Small Particles* (John Wiley & Sons, Inc., New York, 1983).